JGR Solid Earth

RESEARCH ARTICLE
10.1029/2020JB020015

Frictional Strengthening Explored During Non-Steady State Shearing: Implications for Fault Stability and Slip Event Recurrence Time

Matt J. Ikari[1], Brett M. Carpenter[2], Marco M. Scuderi[4], Cristiano Collettini[3,4], and Achim J. Kopf[1]

[1]MARUM Center for Marine Environmental Sciences and Faculty of Geosciences, University of Bremen, Bremen, Germany, [2]School of Geosciences, University of Oklahoma, Norman, OK, USA, [3]Istituto Nazionale di Geofisica e Vulcanologia, Rome, Italy, [4]Dipartimento di Scienze della Terra, Sapienza Universitá di Roma, Rome, Italy

Key Points:
- We analyze friction data from laboratory experiments targeting non-steady state conditions
- Slow loading produces a phase of temporary frictional stability following slip events
- The friction state variable may represent a minimum earthquake recurrence time consistent with natural repeating earthquakes

Supporting Information:
- Supporting Information S1
- Table S1
- Table S2
- Table S3
- Table S4
- Table S5
- Table S6

Correspondence to:
M. J. Ikari,
mikari@marum.de

Citation:
Ikari, M. J., Carpenter, B. M., Scuderi, M. M., Collettini, C., & Kopf, A. J. (2020). Frictional strengthening explored during non-steady state shearing: Implications for fault stability and slip event recurrence time. *Journal of Geophysical Research: Solid Earth*, *125*, e2020JB020015. https://doi.org/10.1029/2020JB020015

Received 22 APR 2020
Accepted 4 OCT 2020
Accepted article online 7 OCT 2020

Abstract On natural faults that host repeating slip events, the inter-event loading time is quite large compared to the slip event duration. Since most friction studies focus on steady-state frictional behavior, the fault loading phase is not typically examined. Here, we employ a method specifically designed to evaluate fault strength evolution during active loading, under shear driving rates as low as 10^{-10} m/s, on natural fault gouge samples from the Waikukupa Thrust in southern New Zealand. These tests reveal that in the early stages of loading following a slip event, there is a period of increased stability, which fades with accumulated slip. In the framework of rate- and state-dependent friction laws, this temporary stable phase exists as long as slip is less than the critical slip distance and the elapsed time is less than the value of the state variable at steady state. These observations indicate a minimum earthquake recurrence time, which depends on the field value of the critical slip distance and the background slip rate. We compare estimates of minimum earthquake recurrence times with the recurrence times of repeating large earthquakes on the Alpine Fault in southern New Zealand and repeating small-magnitude earthquakes on the San Andreas Fault system in California. We find that the observed recurrence times are mostly longer than the predicted minimum values, and exceptions in the San Andreas system may be explained by elevated slip rates due to larger earthquakes in this region.

1. Introduction

Seismogenic faults are known to exhibit a "cycle" of interseismic quiescence punctuated by earthquakes. The nucleation of earthquakes requires that faults become frictionally weaker when shearing at faster rates, a property known as velocity-weakening friction (e.g., Dieterich, 1979, 1981; Scholz, 1998). In order for earthquakes to recur on the same fault patch, the fault strength lost during the earthquake stress drop must be regained during the interseismic period (e.g., Dieterich & Kilgore, 1996). In the last decade, it has become well-documented that faults may also experience various forms of accelerated slip, including slow slip events and low-frequency or very low frequency earthquakes (Ide et al., 2007; Peng & Gomberg, 2010). These also result in stress drops that must be recovered, although they tend to be smaller than stress drops in ordinary earthquakes (Brodsky & Mori, 2007).

In the laboratory, a material's potential for earthquake nucleation is determined by investigating the velocity dependence of friction via the velocity step test, in which the steady-state frictional strengths before and after a sudden change in slip rate are compared (Dieterich, 1979, 1981). The process of strength recovery between earthquakes is simulated with the slide-hold-slide (SHS) test, during which shearing at a constant rate is interrupted by periods of nominally zero driving rate, where the experimental fault is held under quasi-stationary contact (e.g., Carpenter et al., 2016; Dieterich, 1972; Marone & Saffer, 2015). By varying the duration of the "hold" portion of the test, during which the apparatus driving rate is reduced to zero, time-dependent strengthening of the fault can be isolated and measured upon reshear. The SHS test has been instrumental in demonstrating the role of contact aging in frictional slip (e.g., Baumberger & Caroli, 2006; Beeler et al., 1994; Carpenter et al., 2016; Dieterich & Kilgore, 1994; Ikari, Carpenter, & Marone, 2016) and has also been used to understand patterns of recurrence and stress drop in earthquake sequences (Marone, 1998a; Marone et al., 1995; Vidale et al., 1994).

The results of velocity step and SHS tests have in many cases been successfully used to describe earthquakes and the seismic cycle, primarily in numerical simulations (e.g., Ampuero & Rubin, 2008; Avouac, 2015; Barbot et al., 2012; Cao & Aki, 1986; Dieterich, 1992; Okubo, 1989; Roy & Marone, 1996). Despite this, there are some specific shortcomings associated with these tests. For velocity step tests, a fundamental requirement to evaluate frictional stability is that the state variable, representing the lifetime of an asperity population, and the friction coefficient attain a steady-state condition at both the pre-step sliding velocity V_o and the post-step sliding velocity V. On natural plate boundary faults, the stress drop during earthquakes happens very rapidly, so that faults are being actively loaded by tectonic driving forces for all but a very small fraction of time (e.g., Sibson, 1989). Faults that exhibit slow earthquakes also experience loading over the majority of time, as indicated by geodetic measurements showing that the slip during these events occurs over a small portion of the time series (e.g., Dragert et al., 2001; Hirose & Obara, 2005; Linde et al., 1996; Szeliga et al., 2008). Non-steady state friction during the interseismic period and its effect on fault strength and stability may arise not only from plate tectonic loading (as we investigate here) but also from variations in normal stress which are important during both interseismic loading and right after an event (Dieterich & Linker, 1992; Hong & Marone, 2005; Linker & Dieterich, 1992; Richardson & Marone, 1999).

In the case of SHS tests, time-dependent strengthening, also known as frictional healing, is measured for the specific case of zero nominal driving velocity. Natural faults, such as those forming plate boundaries, are remotely loaded by approximately constant driving velocities and thus have a different boundary condition (Chapple & Tullis, 1977; DeMets et al., 1990, 2010). Because the shear stress during the interseismic period is continuously increasing, its effect on frictional healing and how fault strength evolves after the stress drop needs to be addressed. By controlling the shear stress magnitude during SHS tests, previous studies have shown that frictional healing is strongly affected by the magnitude of applied constant shear stress (Karner & Marone, 2001; Ryan et al., 2018) and that during the imposed quasi-static hold, the fault continues to creep at a rate that is dictated by the state evolution and elastic unloading of the apparatus (Beeler et al., 1994). Inducing shear loading with a constant and controlled driving rate, with values approaching plate motion (e.g., Ikari & Kopf, 2017), would further advance the understanding of frictional stability.

We identify here the need for laboratory experiments that can evaluate fault frictional properties under the specific condition of being perturbed when the fault is being remotely loaded but not at steady state. Because major faults are being driven at plate tectonic rates on the order of cm/yr (DeMets et al., 1990, 2010), these experiments need to be conducted at realistically slow driving rates. We develop here a hybrid between SHS and velocity step tests by employing a small (as low as 10^{-10} m/s) shear driving rate rather than zero driving rate during the "hold" portion of the tests, which we term a "velocity cycling" (VC) test. As a first example, we perform VC tests on an outcrop sample of the Waikukupa Thrust, an inactive member of the Alpine Fault system in southern New Zealand (e.g., Boulton et al., 2012; Norris & Cooper, 1997). We then compare the results of VC tests with results from standard SHS and velocity step tests and evaluate their combined implications for fault slip behavior in general.

2. Experimental Methods

For our experiments, we test a natural fault gouge sample collected from a surface exposure of the Waikukupa Thrust, a 4 km long segment of the Alpine Fault on the South Island of New Zealand (Figure 1). It is estimated to have been abandoned approximately 20,000 years BP as active slip transitioned to the Hare Mare imbricate thrust (Norris & Cooper, 1997). The Waikukupa Thrust is located approximately 25 km to the south of the Deep Fault Drilling Project (DFDP) 1A/1B boreholes through the Alpine Fault proper (Toy et al., 2015). The mineral composition of our sample is quantified by X-ray diffraction (XRD) as 25% quartz, 16% feldspar, 14% calcite, and 28% illite + chlorite + mixed layer clay minerals (all other species occur in <4% abundance) (see Vogt et al., 2002 for details on the XRD measurement). Our XRD results are very similar to XRD measurements of fault gouge samples from the DFDP1 boreholes (Boulton et al., 2014; Toy et al., 2015).

For shearing tests, the sample was air-dried, crushed, and sieved to a grain size < 125 μm. The powder was mixed with deionized water to form a stiff paste and pressed into an annular cell volume with an outer diameter of 50 mm, inner diameter of 20 mm, and height of 5 mm, sandwiched between grooved porous metal surfaces. The cell was loaded in a modified Wykeham Farrance-Bromhead ring shear apparatus

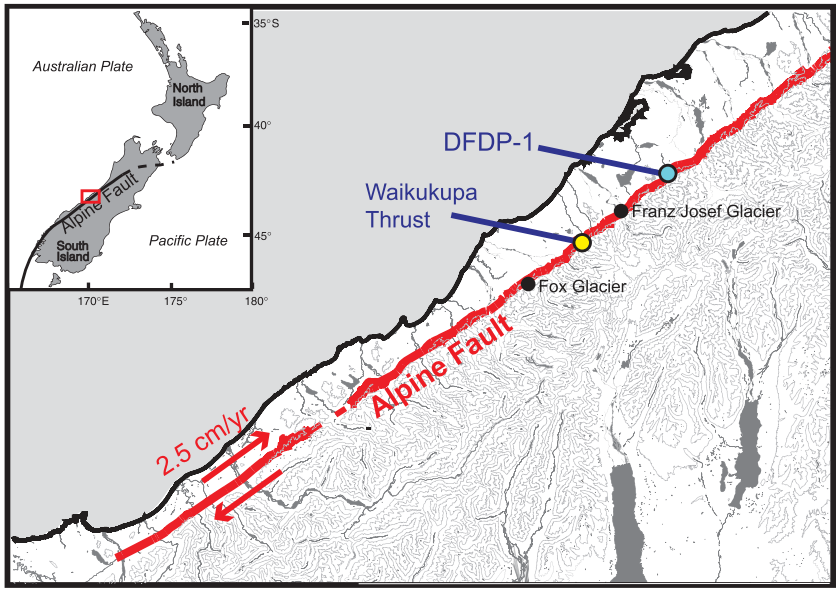

Figure 1. Map showing the location of the Waikukupa Thrust in the western South Island, New Zealand. Locations of the DFDP-1 boreholes shown for reference. Modified from Toy et al. (2015).

(Bishop et al., 1971; Ikari, Carpenter, Vogt, & Kopf, 2016; Kopf, 2013), within which the lower cell holder is driven by an electric stepper motor while the top of the cell is held stationary by two load sensors, which measure the torque provided by the sample resistance. Each load sensor has a resolution of better than 0.09 kPa. Normal load is applied by a dead weight and lever arm; for our experiments, we applied a normal load of 4 MPa, under which most samples compacted to ~3–4 mm. Although the pore pressure is not controlled, the loaded sample was allowed to drain overnight so that the sample height reaches a constant value. We therefore assume negligible excess fluid pressure and that the effective normal stress equals the applied normal stress. The sample was submerged in a bath of deionized water and sheared under fluid-saturated conditions at ~20°C. The sample displacement is designed to be measured from the angular rotation rate indicated by a dial on the rotating stage. Although this measurement is appropriate for shear rates of ≥1 μm/s, at which appreciable displacement accumulates, we also employed here shearing rates as low as 0.1 nm/s (calculated at the midpoint between the inner and outer diameters). These low rates produce displacements too small to be measured by the stage dial during the experiments; therefore, we have verified these low slip rates in our device with a laser displacement sensor (see supporting information).

We initially sheared the samples at a constant velocity of 10 μm/s for at least 30 mm to reach a steady-state residual strength. We continuously measured the shear stress (τ) and calculated an apparent coefficient of sliding friction (μ) as

$$\tau = \mu\sigma_n' \tag{1}$$

where σ_n' is the effective normal stress on the sample and the shear stress includes any effects of cohesion. For standard SHS tests, we employed hold times of 10 to 10^6 s and measured the change in friction $\Delta\mu$ as the difference between the steady-state friction values immediately prior to each individual hold and the peak in friction observed upon re-initiation of shear following the hold (Figure 2a). We evaluate $\Delta\mu$ as a function of time t (Carpenter et al., 2016; Dieterich, 1972) as

$$\Delta\mu = \beta \log(t) \tag{2}$$

where β is the time-dependent strengthening rate, or the rate of frictional healing (decade^{-1}).

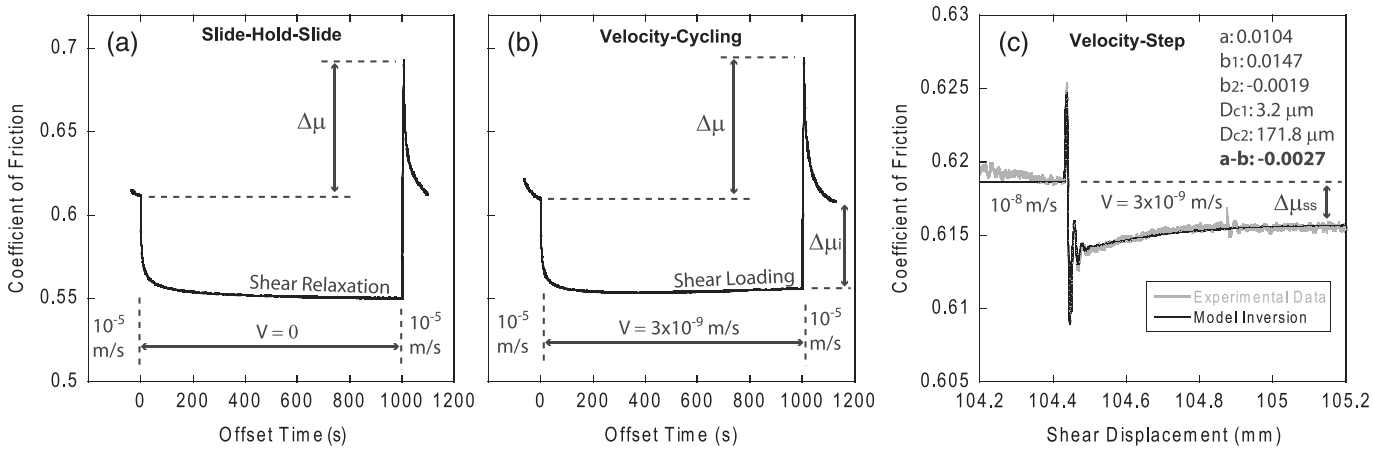

Figure 2. Example of data from a typical experiment, showing (a) at typical slide-hold-slide (SHS) test, (b) a velocity cycling (VC) test, and (c) a standard (threefold velocity increase) velocity step overlain by an inverse model. Note the difference in slope at the end of the 1,000-s period between (a) and (b); also note the distinction between the three quantities $\Delta\mu$, $\Delta\mu_i$, and $\Delta\mu_{ss}$.

Our VC tests were designed to represent a hybrid between standard velocity step and SHS tests. They differ from SHS in that we did not apply a driving rate of 0, but rather very low driving rates of 10^{-10} to 3×10^{-7} m/s, which we refer to here as the inter-cycle velocity. They also differ from standard velocity step in that the friction during these low driving rates may not necessarily reach steady state, and also the velocity change is much larger than most velocity steps. After the change to the lower velocity in VC tests, there is an initial rapid relaxation due to the large velocity change that is similar to SHS tests. A key difference between SHS and VC tests is that the friction (or shear stress) continues to relax throughout the hold period in an SHS test, whereas during the VC tests, shear loading takes over after a characteristic distance or time (Figure 2).

The relaxation in SHS tests (and our VC tests) is controlled by the apparatus stiffness (Beeler et al., 1994), which for the apparatus we employ here is ~4 MPa/mm. In our experiments, we neglect stiffness effects because our experiments were conducted in the same apparatus under consistent conditions (normal stress, background velocity) so the stiffness affected each test equally. Furthermore, we consider the slip that occurs as creep during relaxation to be fundamentally different than the driving slip we employ during the VC tests. This is because during relaxation, slip accumulation occurs when the sample is moving away from steady state. Slip during active loading, even a small amount, occurs as the sample is being driven toward steady state (toward shear failure). It is the effect of slip during active loading, driving the sample toward steady state, that we focus on in our experiments. For example, in Figure 2, we show that the effect of active sliding is to increase the shear stress (or friction) in contrast to an ordinary hold, during which the shear stress (or friction) continually decreases. The effect is quite clear despite the small amount of driving slip (3 μm) at the inter-cycle velocity of 3×10^{-9} m/s shown here.

We measured $\Delta\mu$ in VC tests in the same manner as the SHS tests, from the difference between the steady-state value of μ before the inter-cycle portion of the test and the peak value after resuming shear at the background velocity. Unlike the SHS tests, the $\Delta\mu$ measurements from our VC tests were evaluated over a range of inter-cycle velocities rather than time increments. We performed most VC tests with a constant inter-cycle time of 1,000 s, with a subset of tests at a constant inter-cycle time of ~350,000 s.

For standard velocity step tests, we employed threefold increases in the driving velocity (V) from an initial value (V_o) within the range 10^{-10} to 10^{-4} m/s to measure the velocity dependence of friction. The response of friction to a change in slip velocity is described empirically by a set of equations known as rate-and-state friction (RSF) laws, which for two state variables are written as (Dieterich, 1979, 1981; Reinen et al., 1994)

$$\mu = \mu_o + a \ln\left(\frac{V}{V_o}\right) + b_1 \ln\left(\frac{V_o \theta_1}{D_{c1}}\right) + b_2 \ln\left(\frac{V_o \theta_2}{D_{c2}}\right) \quad (3)$$

$$\frac{d\theta_i}{dt} = 1 - \frac{V\theta_i}{D_{ci}},\ \mathrm{i} = 1,\ 2 \tag{4}$$

where a, b_1, and b_2 are dimensionless parameters, θ_1 and θ_2 are state variables (units of time), and D_{c1} and D_{c2} are critical slip distances over which friction evolves to a new steady-state value (Dieterich, 1979, 1981). In order to extract these parameters, we fit our experimental friction data with an inverse model that combines Equations 3 and 4 and an expression for system stiffness (Reinen & Weeks, 1993; Saffer & Marone, 2003; Skarbek & Savage, 2019) (Figure 2c). We employ the two state variable version of Equations 3 and 4 (defining $b = b_1 + b_2$) (Blanpied et al., 1998; Reinen & Weeks, 1993), which for our data provides a better fit to the data than using one state variable. In particular, the one-state variable model tends to underestimate the peak in friction, overestimate D_c (as compared to D_{c1} in the two-state variable model), and overestimate a-b (see supporting information). Commonly, experimental friction data are superimposed by a small background trend of slip hardening or slip weakening (e.g., Blanpied et al., 1998; Ikari et al., 2013). When modeling our experimental data, we remove these long-term slip-dependent friction trends (e.g., Skarbek & Savage, 2019) as needed in order to avoid biasing and to separate the friction velocity dependence from effects of friction slip dependence (Ikari et al., 2013; Ito & Ikari, 2015).

Equation 4 describes the evolution of the state variable θ and is known as the "Dieterich" or "aging" law, which allows for purely time-dependent changes in friction (Beeler et al., 1994; Dieterich, 1986, 1992). For comparison, we also modeled our data using another state evolution law known as the "Ruina" or "slip" law (Ruina, 1983):

$$\frac{d\theta_i}{dt} = -\frac{V\theta_i}{D_{ci}} ln\left(\frac{V\theta_i}{D_{ci}}\right),\ \mathrm{i} = 1,\ 2. \tag{5}$$

Unlike the aging law, the slip law dictates that friction can only evolve with non-zero slip. Numerical modeling studies have indicated that the choice between the aging and slip laws depends on its application (Bhattacharya et al., 2015; Sleep, 2005, 2006, 2012). The Dieterich aging law is supported by previous studies performing SHS frictional healing experiments (Beeler et al., 1994; Ikari, Carpenter, & Marone, 2016) and by observations of time-dependent increases in real area of contact at contact asperities during static loading (Dieterich & Kilgore, 1994, 1996; Goldsby et al., 2004). The slip law, on the other hand, is supported by some recent studies (Bhattacharya et al., 2017), with a specific application being large changes in sliding velocity (Bhattacharya et al., 2015).

For steady-state sliding at both V and V_o, Equation 3 combined with either Equation 4 or 5 reduces to

$$a - b = \frac{\Delta\mu_{ss}}{\Delta \ln V} \tag{6}$$

where $\Delta\mu_{ss}$ is the change in steady-state friction following the velocity step. The velocity-dependent friction parameter a-b is critical for evaluating the slip behavior of faults because the nucleation of unstable slip that results in earthquake rupture requires a negative value of a-b (i.e., velocity-weakening friction), in combination with specific elastic conditions in the fault surroundings (e.g., Dieterich, 1986, 1992; Dieterich & Kilgore, 1996; Leeman et al., 2016; Marone, 1998b; Scholz, 1998).

In our VC tests, the response of friction from the inter-cycle rate to the background sliding rate can also be evaluated as a velocity step (Figure 5). The key difference between the VC tests and standard velocity steps is that due to the prescribed time window and very low slip rates during the inter-cycle portion of the VC test, steady state is not necessarily reached at the inter-cycle velocity. Because real faults will be perturbed regardless of whether they have attained steady state or not, this condition of initially non-steady state behavior is a specific focus of this study. For example, during afterslip sequences, the fault is shearing at a non-steady state, being in a transient stage between a large velocity perturbation (i.e., earthquake slip) and a slow return to a frictional strength recovery driven by remote tectonic loading. In this case, the conventional RSF laws do not fully characterize these conditions, because the constitutive parameters must be calculated when θ_o and θ, and therefore the friction coefficients at V_o and V, are at steady state (Equation 6). Therefore, we use an alternative but comparable metric specifically for velocity-dependent friction at an initially non-steady state condition:

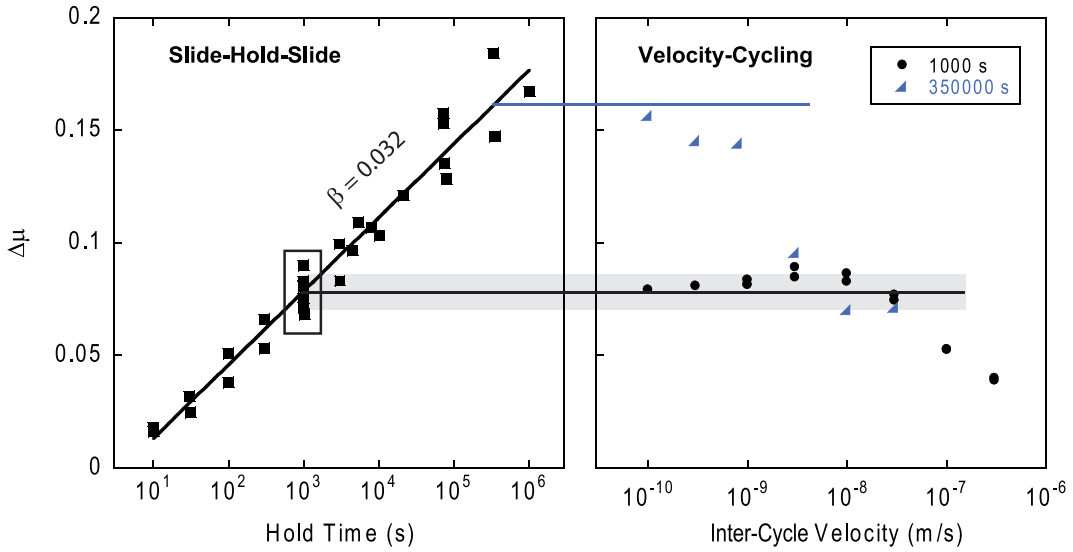

Figure 3. (a) Results of standard slide-hold-slide (SHS) friction tests and (b) results of velocity cycling (VC) friction tests for inter-cycle periods of 1,000 and 350,000 s. Black line is the average $\Delta\mu$ of six 1,000-s holds (black box in panel a); gray shaded area shows the standard deviation of these six $\Delta\mu$ values.

$$\Gamma = \frac{\Delta\mu_i}{\Delta \ln(V)} \tag{7}$$

Here $\Delta\mu_i$ is defined as $\mu(V)_{ss} - \mu_i$, where μ_i is the instantaneous friction coefficient at the end of the inter-cycle period immediately prior to re-initiation of faster sliding. The parameter μ_i is the reference friction value at the non-steady state condition. $\mu(V)_{ss}$ is the steady-state friction coefficient at V as in Equation 6 (Figure 2). The parameter Γ quantifies an apparent friction velocity dependence, and if steady state happens to have been attained at the point where μ_i is measured, then $\Gamma = a\text{-}b$.

3. Experimental Results

From the standard SHS tests, we measured a healing rate β of 0.032 decade^{-1} (Figure 3). Healing exhibits a log-linear dependence on time for all hold times up to 10^6 s. Multiple measurements were made to demonstrate repeatability; from a set of six measurements of a 1,000-s hold, we calculated a standard deviation of 0.008 in $\Delta\mu$. We performed 1,000-s VC tests for inter-cycle velocities ranging from 10^{-10} (0.1 nm/s, or 3 mm/yr) to 3×10^{-7} m/s (0.3 μm/s). We observe that $\Delta\mu$ for VC tests increases as a function of increasing inter-cycle velocity to maximum values at 3×10^{-9} and 1×10^{-8} m/s. To compare with standard SHS tests, we calculated an average value and standard deviation from the six repeated 1,000-s SHS tests, which we compared to $\Delta\mu$ values from our VC tests (Figure 3). The comparison shows that for inter-cycle velocities of 3×10^{-9} and 1×10^{-8} m/s, $\Delta\mu$ values are higher than the average value of $\Delta\mu = 0.078$ for a standard 1,000-s hold and lie near or above the standard deviation for the 1,000-s holds. $\Delta\mu$ then decreases log-linearly for inter-cycle velocities $\geq 10^{-8}$ m/s. A smaller set of ~350,000-s VC tests with inter-cycle velocities in the range 10^{-10} to 3×10^{-8} m/s show an approximately log-linearly decreasing trend in $\Delta\mu$ with increasing inter-cycle velocity, with no values exceeding the $\Delta\mu$ value expected from a 350,000-s hold.

Standard velocity step tests with threefold velocity increases, evaluated at steady state, show consistently velocity-weakening behavior for V ranging between 10^{-9} and 3×10^{-5} m/s (Figure 4a). Oscillations in friction resembling stick-slip instabilities are observed at velocities of $\leq 3 \times 10^{-9}$ m/s (supporting information), which are consistent with repetitive slow stick-slip observed in a sample of the Alpine Fault under similar conditions (Ikari, 2019). These slip events preclude measurement of $a\text{-}b$ values but allow us to infer velocity-weakening friction at these low driving rates and presumably more velocity-weakening than at higher velocities where the oscillations are absent. In comparison, Γ values (the apparent friction velocity dependence evaluated via Equation 7) obtained from the 1,000-s VC tests show apparent velocity-strengthening behavior when

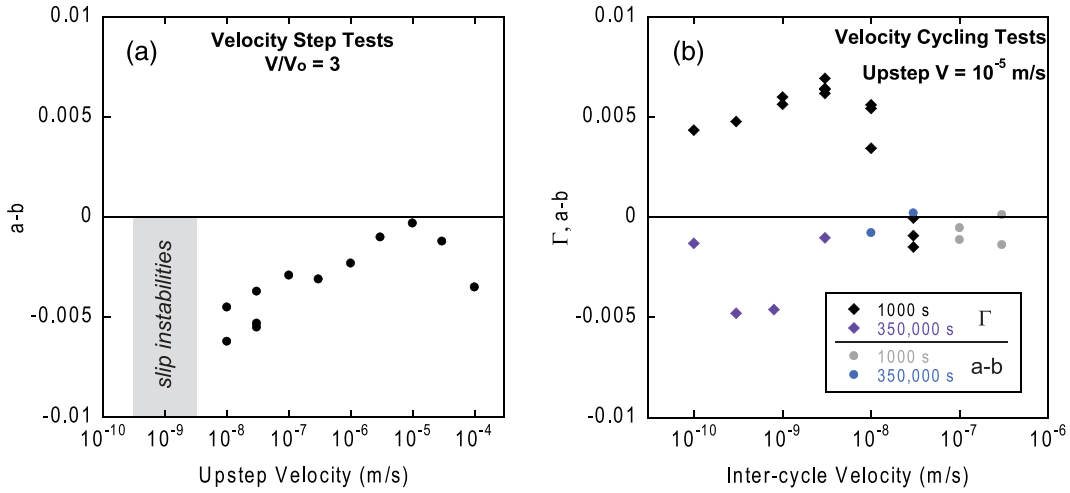

Figure 4. (a) Velocity-dependent friction parameter *a-b* extracted from threefold increases in slip velocity, shown as a function of initial slip velocity. Gray box shows velocity range where frictional oscillations resembling stick-slip occurred, indicating velocity-weakening friction without a determinable *a-b* value. (b) Γ values from 1,000-s VC tests, shown as a function of inter-cycle velocity. For VC tests during which the friction reached steady state, *a-b* values are reported instead of Γ.

the inter-cycle velocity is 10^{-8} m/s or lower and velocity-weakening behavior for inter-cycle velocities above 10^{-8} m/s (Figure 4b). For the 1,000-s VC tests, the Γ values (and therefore $\Delta\mu_i$) exhibit the same pattern as the healing measured as $\Delta\mu$—increasing as a function of increasing inter-cycle velocity to maximum values at 3×10^{-9} and 1×10^{-8} m/s and then decreases log-linearly for inter-cycle velocities $\geq 10^{-8}$ m/s. We note that the velocities at which we observe maximum values in Γ from the 1,000-s VC tests are the same at which we observe a maximum in $\Delta\mu$. Γ values obtained from the ~350,000-s VC tests consistently show (apparent) velocity-weakening friction. For some VC tests (both 1,000 and ~350,000), steady-state is reached; these cases are fit with the inverse model and presented as *a-b* values, which are consistently <0.

Based on our experimental results, we have performed some preliminary simulations using a rate-and-state forward model with one state variable for 1,000-s VC tests and a 1,000-s hold (see supporting information).

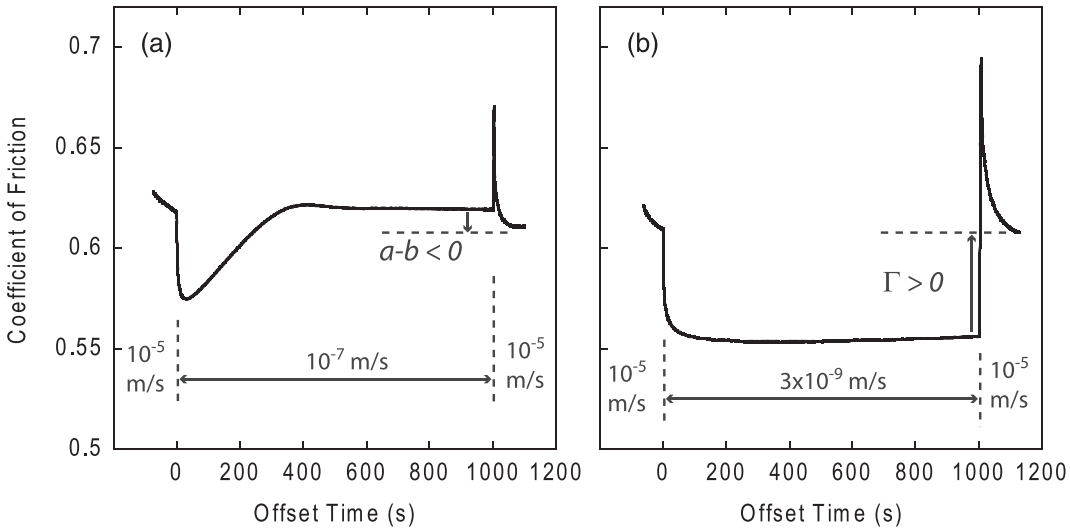

Figure 5. Comparison of (a) a 1,000-s VC test with an inter-cycle velocity of 3×10^{-9} m/s and (b) a 1,000-s VC test with an inter-cycle velocity of 10^{-7} m/s. Note the difference between *a-b* and Γ due the differences in accumulated slip at different rates for a fixed period of 1,000 s.

These predictions generally match the experimental data, including (1) the form of the friction curve during the velocity cycles, (2) the decrease in healing at larger inter-cycle velocities, and (3) the transition from apparent velocity strengthening to apparent (or true) velocity weakening at larger inter-cycle velocities. The aging law provides a better match to the data in some instances, and in other instances, the slip law provides a better match; however, neither law matches our observations exactly. Note that these are preliminary simulations; a more robust analysis requires a more comprehensive modeling study (including simulations using two state variables) that is outside the scope of this experimental study.

4. Role of Displacement During Active Fault Loading

4.1. A Period of Advanced Healing

The comparison between VC tests and SHS tests shows that the non-zero loading rate during the inter-cycle period of the VC tests at 10^{-9} to 10^{-8} m/s tends to induce larger healing on average compared to standard SHS tests. The healing ($\Delta\mu$) values do not clearly extend outside the upper standard deviation range for an ordinary hold, indicating that the presence of additional healing in this velocity range may not be unambiguous. However, given that the VC healing values are consistently larger than the average value for the 1,000-s hold and that two data points do exceed the standard deviation for an ordinary hold (at inter-cycle velocities of 3×10^{-9} and 10^{-8} m/s), we must acknowledge the possibility of additional healing during shear loading. Simulations (see supporting information) using the slip law predict increased healing within a limited velocity range, similar to what we observe; however, the aging law does not predict increased healing.

If additional healing occurs, it is related to the active shear loading during the VC tests. Healing from conventional SHS tests is explained by volumetric strain at grain-scale contact asperities, driven by the normal load and therefore in 1-D. When the sample is also experiencing shear loading, this adds an additional component of lateral compaction via grain rolling and sliding. This lateral compaction is driven by sub-failure shear loading rather than active shearing following failure and is similar to "shear-enhanced compaction" observed in sands and sandstones (Baud et al., 2006; Cashman & Cashman, 2000). However, the extra healing is clearly limited; at inter-cycle velocities $> 10^{-8}$ m/s, healing clearly decreases below the standard SHS value (Figure 3). This is because slip at higher velocities causes a decrease in contact area, affecting healing (e.g., Marone, 1998b). Therefore, this signifies a transition from healing being facilitated by sub-failure shear loading to healing being disrupted by dilatancy associated with shear failure (Marone et al., 1990; Teufel, 1981), due to larger accumulated displacement (i.e., for a fixed inter-cycle amount of time the displacement increases as the velocity increases).

Additional healing is not observed for inter-cycle velocities lower than ~10^{-9} m/s, likely because these rates are too slow to induce sufficient shear loading within 1,000 s so that the gouge is still in a state of relaxation similar to standard SHS tests. If the slip from driving is sufficiently small—either due to low elapsed time or very slow driving rates—then the signal from active driving would be overwhelmed by creep due to the relaxation of the sample and apparatus. This can be seen in our data, where the initial shape of the friction curve for both a standard hold and low inter-cycle velocity is very similar (Figure 2). However, relaxation creep rate decreases with time, whereas the loading rate is constant. Therefore, with increasing time, the effect of shear loading takes over and tends to dominate over the relaxation, with the time necessary to see the effect of shear loading being longer for slower inter-cycle velocities. This is consistent with forward models of our velocity cycle tests (see supporting information), which suggest that the slip rate at the end of a 1,000-s velocity cycle is comparable to that at the end of an ordinary hold for inter-cycle velocities of $\leq 10^{-9}$ m/s; but for inter-cycle velocities $> 10^{-9}$ m/s, the slider velocity during the cycle is higher than the end velocity in an ordinary hold. This supports our explanation for the observed higher healing, because higher healing is observed for velocity cycle tests during which the slip velocity is always larger than the velocity at the end of an ordinary hold. It is also observed that the slip law reproduces advanced healing, supporting the idea that active shearing plays an important role.

4.2. Temporarily Enhanced Frictional Stability

The displacement that accumulates during the inter-cycle period also plays an important role in frictional stability. We observe consistent steady-state velocity-weakening friction from our conventional velocity step

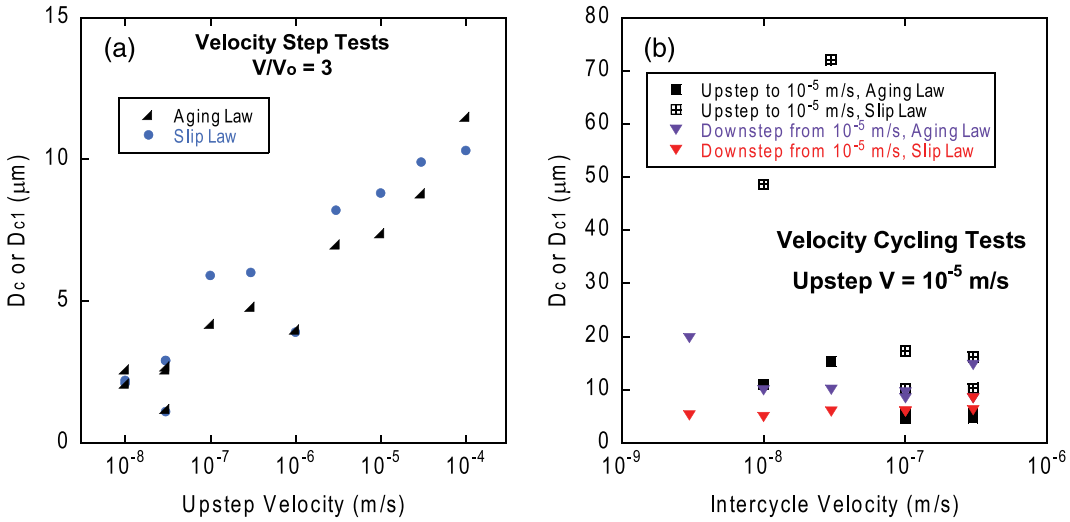

Figure 6. Critical slip distance as a function of (a) inter-cycle velocity during VC tests and (b) upstep slip velocity from velocity step tests with a threefold velocity increase.

tests; however, our VC tests exhibit apparent velocity-strengthening as well as weakening depending on inter-cycle velocity. Apparent velocity-strengthening values are observed for VC tests with the shorter inter-cycle times (1,000 s) and slower inter-cycle velocities ($\leq 10^{-8}$ m/s), which contrast with (1) apparent velocity weakening observed for the longer inter-cycle times of ~350,000 s and (2) true velocity-weakening observed for 1,000-s cycles and inter-cycle velocities of $\geq 10^{-7}$ m/s (Figure 4b). We illustrate this by comparing 1,000-s VC tests with inter-cycle velocities of 3×10^{-9} and 10^{-7} m/s (Figure 5). The friction coefficient in the VC test with the faster inter-cycle velocity reaches steady state; therefore, an a-b value can be extracted which is negative. On the other hand, at the slower inter-cycle velocity, steady state is not reached and Γ must be calculated, which in this case is positive indicating apparent velocity strengthening. The inter-cycle driving slip at 1,000 s is 100 μm at 10^{-7} m/s and 3 μm at 3×10^{-9} m/s; therefore, whether strengthening or weakening occurs depends on whether steady state is reached after the inter-cycle portion of the test, suggesting that it depends on whether the critical slip distance is exceeded.

To test the role of D_c, their values must be known for the inter-cycle velocities. Since D_c must be extracted from RSF constitutive modeling, they can only be determined directly from VC tests if the inter-cycle friction coefficient reaches steady state. Because we used two state variables to fit our data, we consider D_{c1} rather than D_{c2} for two main reasons: (1) D_{c1} corresponds with b_1, which characterizes the strength decrease immediately following the direct effect and is therefore most relevant for slip event nucleation, and (2) D_{c1} is significantly shorter than D_{c2} (supporting information) and can be used as a lower bound; since frictional stability is inversely related to D_c (Scholz, 1998), this represents a conservative estimate. We observe no clear difference between D_c values obtained using the aging or slip laws within a certain amount of data scatter (Figure 6); therefore, we use D_c values determined with Dieterich's aging law for the remainder of our analyses.

D_c could be directly determined for our fastest VC tests, which reached steady state for inter-cycle velocities of 10^{-7} and 3×10^{-7}m/s (1,000 s) and 10^{-8} and 3×10^{-8}m/s (~350,000 s). For lower inter-cycle velocities, the data could not be fit with the RSF model, either due to insufficient accumulated slip (in 1,000-s VC tests), or in some cases because of stick-slip-like oscillations obscuring steady state (supporting information). For these VC tests, we retrieve a value of D_c by either (1) for 1,000-s VC tests, assuming a D_c value from a ~350,000-s VC test with the same inter-cycle velocity, or (2) assuming a value of 10 μm as a representative value (Figure 6).

By converting the driving rate to an amount of inter-cycle displacement δ, we can compare this displacement value against the critical slip distance for each of our VC tests. We observe apparent velocity strengthening ($\Gamma > 0$) when the inter-cycle slip does not exceed the critical slip distance, or when $\delta/D_c \leq 1$. When $\delta/D_c > 1$,

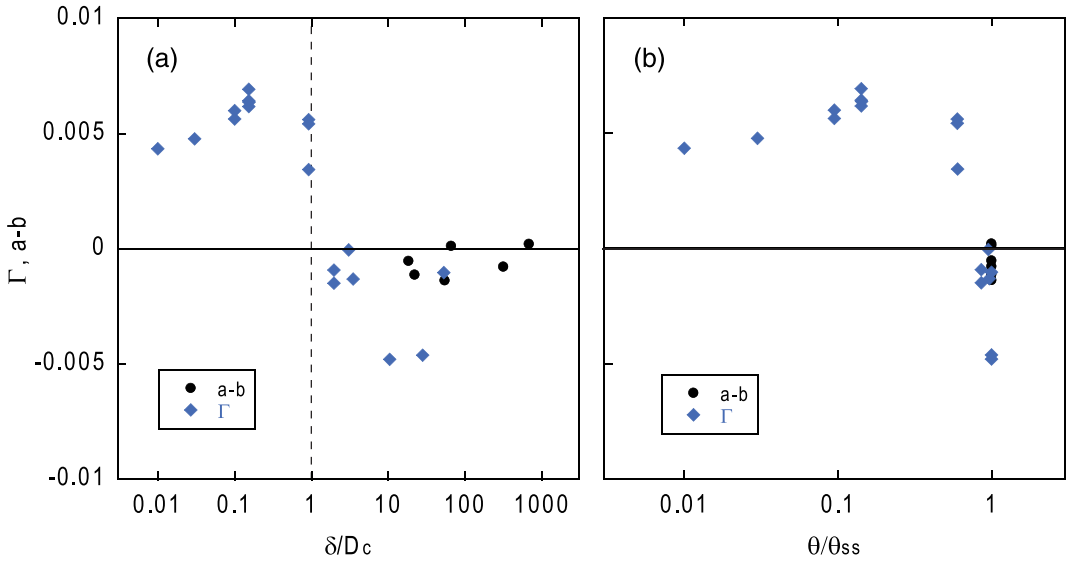

Figure 7. Friction velocity dependence as a function of (a) δ/D_c and (b) θ/θ_{ss}, shown as a-b for VC tests during which at least 100 μm of slip accumulated during the inter-cycle period and Γ for all other VC tests. For VC tests during which the friction reached steady state, a-b values are reported instead of Γ.

predominantly velocity weakening is observed (note that when $\delta/D_c > 1$, steady state is reached and $\Gamma = a\text{-}b$) (Figure 7). A similar analysis can be made using the state variable θ (considering θ to be θ_1, as we do with D_c). At steady state, $\theta_{ss} = D_c/V$; when not at steady state, the instantaneous value of θ can be calculated as

$$\theta = \frac{D_c}{V} + \left(\theta_o - \frac{D_c}{V}\right) e^{-\delta/D_c} \tag{8}$$

(Dieterich, 1992), where θ_o is the state variable at V_o ($\theta_o = D_c/V_o$). Our data show that apparent velocity strengthening ($\Gamma > 0$) is observed when $\theta/\theta_{ss} < 0.95$, and velocity-weakening is dominant when θ/θ_{ss} is ~1 (Figure 7). The largest Γ values are observed for $\delta/D_c = 0.10$–0.14 and $\theta/\theta_{ss} = 0.095$–$0.130$, which are measured for inter-cycle velocities of 10^{-9} and 3×10^{-9} m/s.

These results demonstrate that following a slip event, if the critical slip distance is not reached, the material will strengthen when the fault is perturbed. The fault would resist accelerating slip as if it was a velocity-strengthening material, even if the fault exhibits velocity weakening under steady-state conditions. However, this phase is transient and velocity-weakening behavior resumes once slip exceeds D_c and enough time elapses equivalent to the state variable at steady state (defined by the frictional behavior of the fault material). The effect of this temporary stable phase is largest when the slip is about 10% of D_c and the time elapsed is 10% of the steady-state state variable (Figure 7).

For our 1,000-s VC experiments, the inter-cycle velocities that produce the largest apparent velocity strengthening also produced the largest healing values, exceeding the strengthening observed in standard SHS tests (Figure 3). At these rates (10^{-9} to 10^{-8} m/s), the shear stress is near its lowest value due to relaxation following the slip event (Figure 5). Therefore, the most rapid healing coincides with the point at which the shear stress on the fault is the farthest below its failure strength. Note that this difference between stress and strength is expected to be largest early in the inter-cycle phase, when relaxation transitions to transient loading. This difference between stress and strength contributes to enhancing the temporary frictional stability.

5. Implications of a Temporary Stable Phase Following Slip Events

The potential existence of a period of enhanced stability following slip events holds important implications for spatiotemporal earthquake patterns, with the caveat that the results obtained from our Waikukupa Thrust gouge are assumed to be generally applicable to natural faults. Because we relate our analysis to

the process of repeated cycles of stress drops and reloading, it is implicit that this study is applicable to seismogenic and/or slow slip faults. Our data suggest that frictional instability may be suppressed for a period following a slip event, as is to be expected based on earthquake cyclicity. One implication of the temporary stable phase is that slow afterslip may be expected on a recently slipped fault patch, whereas in numerical simulations, coseismic slip and afterslip are usually considered to occur on adjacent, but different fault patches (e.g., Marone et al., 1991; Miyazaki et al., 2004; Perfettini et al., 2010; Perfettini & Avouac, 2004, 2007). The temporary stable phase may also affect the tendency of slow slip faults to be driven to ordinary earthquake speeds. Using a combination of laboratory friction data and geophysical observations from the Tohoku region of the Japan Trench subduction zone, Ito et al. (2017) suggested that ongoing slow fault slip (in this case, foreshock afterslip) could enhance susceptibility to coseismic slip propagation via a slip-weakening mechanism, provided that sufficiently fast rates are reached. On the other hand, the results of our study indicate enhanced stability via an increase in the apparent velocity dependence of friction following a slip event during shear loading, which is a strain- (or slip-) hardening phase. Therefore, the combined results of Ito et al. (2017) and our study suggest that fault stability can vary over different phases of a slip event cycle. Finally, another important implication which we explore in more detail is its potential effect on earthquake recurrence time.

6. Temporary Frictional Stability and Minimum Earthquake Recurrence Times

6.1. Estimation of Recurrence Times on Natural Faults

In our laboratory experiments, the temporary stable phase depends on D_c as measured from velocity step data; therefore, on natural faults, the stable phase depends on the field value of D_c, which previous studies have shown is several orders of magnitude larger (Griffith & Prakash, 2015; Marone & Kilgore, 1993; Ohnaka, 2003). Combined with measurements of long-term fault slip rate as V, the field value of the state variable at steady-state θ_{ss} is then equivalent to the field value of D_c/V. Since our laboratory data indicate that θ_{ss} is an elapsed time before frictional instability is possible, we suggest that the field value of θ_{ss} represents a minimum recurrence time for repeating earthquakes. In order to calculate the minimum recurrence time, it is necessary to upscale D_c from laboratory values to appropriate field values. Slip during the slow earthquake nucleation phase can be estimated from seismograms (Ellsworth & Beroza, 1995), and this slip amount is conceptually equivalent to the critical slip distance for instability (e.g., Ohnaka, 2000). We therefore use the seismologically determined value of D_c as a proxy for the field value of the laboratory-measured D_c. Seismologically-derived estimates of D_c for earthquakes of M_w between 2.6 and 8.1 (Ellsworth & Beroza, 1995; Ide & Takeo, 1997; Papageorgiou & Aki, 1983) are roughly in the centimeter to meter range. Based on these data, Ohnaka (2000) proposed that D_c exhibits a positive relationship with the seismic moment M_o:

$$M_o = 10^{19} D_c^3 \tag{9}$$

Using this relation, D_c can also be estimated based on earthquake moment magnitude M_w using a standard scaling relation between M_o and M_w:

$$M_w = \frac{2}{3}\log_{10} M_o - 6 \tag{10}$$

for M_o having units of N·m (Kanamori, 1986).

6.2. Application to the Alpine Fault

Although the Waikukupa Thrust itself is currently inactive, it can be considered as an ancient exhumed analogue of the active Alpine Fault, the upper portion of which was recently drilled as part of the DFDP (Sutherland et al., 2012; Toy et al., 2015). The composition of our sample (41% quartz + feldspar, 14% calcite, 36% illite/chlorite/mixed layer clay minerals) is very similar to samples of gouge from one of the two principal slip zones encountered in the DFDP-1B borehole. This includes a sample tested by Boulton et al. (2014) (48% quartz + feldspar, 10% calcite, 32% smectite + illite + muscovite) and another sample tested by Ikari et al. (2014) as well as Ikari and Kopf (2017) (44% quartz + feldspar, 8% calcite, 38% smectite + illite + muscovite + chlorite). XRD data for the Ikari and Kopf (2017) sample were not previously reported; however, we

have quantified the mineral assemblage for that sample using the same method as for the Waikukupa sample. The high friction coefficient measured at the background shearing rate (10 μm/s), velocity-weakening behavior in standard velocity step tests, and large healing rate we observe are consistent with previous measurements on fault gouges from the Alpine Fault itself (Boulton et al., 2014; Ikari et al., 2014, 2015; Ikari & Kopf, 2017; Niemeijer et al., 2016).

The Alpine Fault is considered to be near the end of its earthquake cycle, capable of a M_w 7+ earthquake (e.g., Sutherland et al., 2007; Townend et al., 2009). On the Alpine Fault, the long-term slip rate is ~2.5 cm/yr (Cooper & Norris, 1994; Norris & Cooper, 2000; Sutherland et al., 2006). Using this value and Equations 9 and 10, an earthquake with $M_w = 7$ would have a D_c of 1.5 m and a minimum recurrence time of 59 years, and a $M_w = 8$ would have a D_c of 4.6 m and a minimum recurrence time of 184 years. These values are lower than estimates of the recurrence interval of large earthquakes on the Alpine Fault from paleoseismologic techniques, although they can vary widely. Adams (1980) estimated a recurrence interval of 500 years, whereas Wells et al. (1999) suggested a more irregular recurrence in the range of 100–280 years. Bull (1996) and Berryman et al. (2012) suggest averages of 260 and 330 years, respectively. General consensus is that the last large Alpine Fault earthquake occurred in 1717 AD (De Pascale & Langridge, 2012; Sutherland et al., 2007; Wells et al., 1999). If a minimum recurrence of slightly more than 300 years indicates a D_c of 7.6 m, this suggests that the current Alpine Fault is capable of a $M_w = 8.4$ earthquake or greater, consistent with the assessment of Sutherland et al. (2007).

6.3. Application to the Northern San Andreas Fault System

Although our results were obtained from fault gouge from the Alpine Fault system, the concept of minimum earthquake repeat time based on field values of D_c and θ_{ss} should be applicable to all fault zones, if they obey RSF laws. A more robust comparison can be made with catalogs of repeating earthquakes on the northern San Andreas Fault system, recorded by the CALNET seismic network (Oppenheimer et al., 1992). We investigate here two specific earthquake catalogs: a repeating sequence of M_w ~1.5 earthquakes (named the CA1 sequence) on the Calaveras Fault in the vicinity of the 1984 $M_w = 6.2$ Morgan Hill earthquake (Vidale et al., 1994), and sets of repeating earthquakes classified as doublets, triplets, and one quadruplet (Beroza et al., 1995). These earthquakes have M_w ranging from 1.0 to 2.8 and occurred on the San Andreas, Calaveras, and Sargent faults in the region of the $M_w = 6.9$ Loma Prieta earthquake. A key characteristic of each of these earthquake sets is that they occur on the same fault patch and have the same focal mechanism. The CA1 sequence was used in previous studies applying frictional healing from SHS tests to earthquake recurrence patterns (Marone, 1998a; Marone et al., 1995).

For these repeating earthquakes in the northern San Andreas Fault system, D_c values estimated from M_w using Equations 9 and 10 range from ~1.5 mm to 1.2 cm. The long-term displacement rate on the San Andreas Fault is ~2.5 cm/yr, also similar to the Alpine Fault (Ryder & Bürgmann, 2008; Titus et al., 2005). On the Calaveras Fault, the average slip rate is ~1.5 cm/yr (Working Group on California Earthquake Probabilities, 1999), whereas it is only 0.3 cm/yr on the Sargent Fault (Prescott & Burford, 1976). If the minimum recurrence time calculated as D_c/V represents the minimum time necessary for instability, then the observed recurrence times from the repeating earthquakes should exceed these values. The observed recurrence intervals vary widely, ranging from 1 to over 3,200 days (about 9 years). Most of these values exceed the calculated minimum recurrence, which for M_w of 1–2.5 ranges from 21–120 days for the San Andreas Fault and 36–200 days for the Calaveras Fault. Despite the low offset rate, the recurrence time of the Sargent Fault doublet is nearly an order of magnitude larger than the estimated minimum value.

In some cases, the recurrence is shorter than these minimum estimates (Figure 8a). However, these shorter recurrence intervals occur in the immediate temporal vicinity of larger earthquakes: the 1984 Morgan Hill earthquake on the Calaveras Fault (Bakun et al., 1984) and the 1989 Loma Prieta earthquake on the San Andreas Fault (Dietz & Ellsworth, 1990). We infer that elevated slip rates associated with these earthquakes are therefore responsible for the shorter observed recurrence by increasing V relative to D_c (Figure 8b). Based on the estimated D_c values, slip rates were elevated to at least 37 cm/yr following both the Morgan Hill and Loma Prieta earthquakes, consistent with earthquake afterslip in the area (Segall et al., 2000). For the Loma Prieta earthquake, the largest slip rate on the San Andreas Fault of at least 94 cm/yr occurred before the mainshock. This suggests precursory slip prior to the Loma Prieta earthquake, which is consistent with

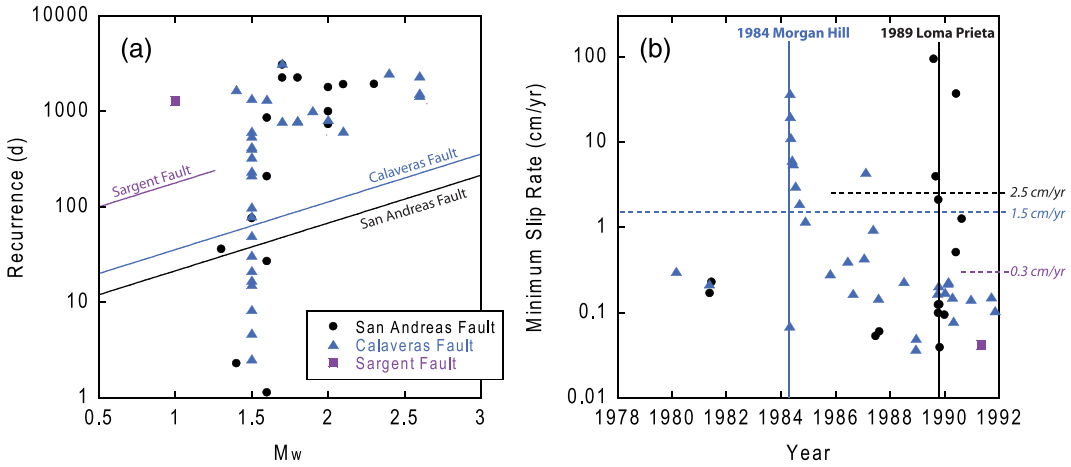

Figure 8. (a) Recurrence time (days) for a catalog of earthquake multiplets (Beroza et al., 1995) and the CA1 earthquake sequence (Vidale et al., 1994) on the northern San Andreas Fault, Calaveras Fault, and Sargent Fault, California. Solid slanted lines show the minimum recurrence interval calculated as $\theta = D_c/V$, where D_c is obtained from M_w following Ohnaka (2000) and V is 2.5 cm/yr for the San Andreas Fault, 1.5 cm/yr for the Calaveras Fault, and 0.3 cm/yr for the Sargent Fault. (b) Minimum slip rates calculated for the two earthquake catalogs, assuming $\theta = D_c/V$ represents the minimum recurrence. Timing of the $M_w = 6.2$ Morgan Hill and $M_w = 6.9$ Loma Prieta earthquakes, as well as the long-term slip rates for the three faults are shown for reference.

observations of elevated seismic activity and thus elevated stress and strain (Bowman & King, 2001). As a final caveat, we note that the above analysis is based on strictly friction mechanics considerations. Although friction alone can explain the observational data, other mechanisms such as pore pressure fluctuations and distribution can clearly affect earthquake timing. One example of this is the Alto Tiberina fault in the northern Appenines, Italy, where rapidly recurring earthquakes are related to CO_2 overpressuring (Chiaraluce et al., 2007; Miller et al., 2004).

7. Conclusions

We develop and utilize a method of laboratory friction testing called a velocity-cycling (VC) test, which is a modified version of the SHS test employing a very low driving velocity during the "hold" portion of the test. The VC test is applicable to periods of transient fault loading and therefore probably represents the state of most major faults over a majority of the time. We use a natural fault gouge outcrop sample from the Waikukupa Thrust, an abandoned strand of the Alpine Fault system in New Zealand. Standard velocity stepping and SHS tests show that this sample is strong and tends toward frictional instability, consistent with other fault gouges from the Alpine Fault. Our VC tests show that slow but non-zero shearing rates may induce larger healing than in conventional SHS tests via active shear loading. Importantly, the VC tests also reveal that during transient loading, our sample exhibits a temporary phase of frictional stability that fades with accumulating displacement and vanishes when the critical slip distance is exceeded and enough time has elapsed to match the steady-state value of the state variable. This observation suggests that frictional stability evolves with position in the slip event cycle and that a minimum repeat time for rupturing fault patches may exist, which is defined by the field values of D_c and θ_{ss}. This is supported by the recurrence times of repeating earthquakes in the northern San Andreas Fault system which are mostly longer than the minimum times estimated from field values of D_c; shorter recurrence times coincide temporally with large earthquakes in the region and may therefore be a consequence of locally elevated slip rates.

Data Availability Statement

All data are available from the Pangaea data publisher for earth and environmental science (https://doi.pangaea.de/10.1594/PANGAEA.915079).

Acknowledgments

This work was supported by the Deutsche Forschungsgemeinschaft via MARUM Research Centre/Cluster of Excellence (grants FZT15, EXC309, and IK 107/3-1) and from the European Research Council (ERC) under the European Union's Horizon 2020 research and innovation program (grant agreement 714430) to M. I.

References

Adams, J. (1980). Paleoseismicity of the Alpine Fault seismic gap, New Zealand. *Geology*, *8*, 72–76. https://doi.org/10.1130/0091-7613(1980)8<72:POTAFS>2.0.CO;2

Ampuero, J.-P., & Rubin, A. M. (2008). Earthquake nucleation on rate and state faults—Aging and slip laws. *Journal of Geophysical Research*, *113*, B01302. https://doi.org/10.1029/2007JB005082

Avouac, J.-P. (2015). From geodetic imaging of seismic and aseismic fault slip to dynamic modelling of the seismic cycle. *Annual Review of Earth and Planetary Sciences*, *43*(1), 233–271. https://doi.org/10.1146/annurev-earth-060614-105302

Bakun, W. H., Clark, M. M., Cockerham, R. S., Ellsworth, W. L., Lindh, A. G., Prescott, W. H., et al. (1984). The 1984 Morgan Hill, California, earthquake. *Science*, *225*(4659), 288–291. https://doi.org/10.1126/science.225.4659.288

Barbot, S., Lapusta, N., & Avouac, J.-P. (2012). Under the hood of the earthquake machine: Toward predictive modelling of the seismic cycle. *Science*, *336*(6082), 707–710. https://doi.org/10.1126/science.1218796

Baud, P., Vajdova, V., & Wong, T.-F. (2006). Shear-enhanced compaction and strain localization: Inelastic deformation and constitutive modeling of four porous sandstones. *Journal of Geophysical Research*, *111*, B12401. https://doi.org/10.1029/2005JB004101

Baumberger, T., & Caroli, C. (2006). Solid friction from stick-slip down to pinning and aging. *Advances in Physics*, *55*(3–4), 279–348. https://doi.org/10.1080/00018730600732186

Beeler, N. M., Tullis, T. E., & Weeks, J. D. (1994). The roles of time and displacement in the evolution of rock friction. *Geophysical Research Letters*, *21*(18), 1987–1990. https://doi.org/10.1029/94GL01599

Beroza, G. C., Cole, A. T., & Ellsworth, W. L. (1995). Stability of coda wave attenuation during the Loma Prieta, California, earthquake sequence. *Journal of Geophysical Research*, *100*(B3), 3977–3987. https://doi.org/10.1029/94JB02574

Berryman, K. R., Cochran, U. A., Clark, K. J., Biasi, G. P., Langridge, R. M., & Villamor, P. (2012). Major earthquakes occur regularly on an isolated plate boundary fault. *Science*, *336*(6089), 1690–1693. https://doi.org/10.1126/science.1218959

Bhattacharya, P., Rubin, A. M., Bayart, E., Savage, H. M., & Marone, C. (2015). Critical evaluation of state evolution laws in rate and state friction: Fitting large velocity steps in simulated fault gouge with time-, slip- and stress-dependent constitutive laws. *Journal of Geophysical Research: Solid Earth*, *120*, 6365–6385. https://doi.org/10.1002/2015JB012437

Bhattacharya, P., Rubin, A. M., & Beeler, N. M. (2017). Does fault strengthening in laboratory rock friction experiments really depend primarily upon time and not slip? *Journal of Geophysical Research: Solid Earth*, *122*, 6389–6430. https://doi.org/10.1002/2017JB013936

Bishop, A. W., Green, G. E., Garga, V. K., Andresen, A., & Brown, J. D. (1971). A new ring shear apparatus and its application to the measurement of residual strength. *Geotechnique*, *21*(4), 273–328. https://doi.org/10.1680/geot.1971.21.4.273

Blanpied, M. L., Marone, C. J., Lockner, D. A., Byerlee, J. D., & King, D. P. (1998). Quantitative measure of the variation in fault rheology due to fluid-rock interactions. *Journal of Geophysical Research*, *103*(B5), 9691–9712. https://doi.org/10.1029/98JB00162

Boulton, C., Carpenter, B. M., Toy, V. G., & Marone, C. (2012). Physical properties of surface outcrop cataclastic fault rocks, Alpine Fault, New Zealand. *Geochemistry, Geophysics, Geosystems*, *13*, Q01018. https://doi.org/10.1029/2011GC003872

Boulton, C., Moore, D. E., Lockner, D. A., Toy, V. G., Townend, J., & Sutherland, R. (2014). Frictional properties of exhumed fault gouges in DFDP-1 cores, Alpine Fault, New Zealand. *Geophysical Research Letters*, *41*, 356–362. https://doi.org/10.1002/2013GL058236

Bowman, D. D., & King, G. C. P. (2001). Accelerating seismicity and stress accumulation before large earthquakes. *Geophysical Research Letters*, *28*(21), 4039–4042. https://doi.org/10.1029/2001GL013022

Brodsky, E. E., & Mori, J. (2007). Creep events slip less than ordinary earthquakes. *Geophysical Research Letters*, *34*, L16309. https://doi.org/10.1029/2007/GL030917

Bull, W. B. (1996). Prehistorical earthquakes on the Alpine Fault, New Zealand. *Journal of Geophysical Research*, *101*(B3), 6037–6050. https://doi.org/10.1029/95JB03062

Cao, T., & Aki, K. (1986). Seismicity simulation with a rate- and state-dependent friction law. *Pure and Applied Geophysics*, *124*, 487–513. https://doi.org/10.1007/978-3-0348-6601-9_6

Carpenter, B. M., Ikari, M. J., & Marone, C. (2016). Laboratory observations of time-dependent frictional strengthening and stress relaxation in natural and synthetic fault gouges. *Journal of Geophysical Research: Solid Earth*, *121*, 1183–1201. https://doi.org/10.1002/2015JB012136

Cashman, S., & Cashman, K. (2000). Cataclasis and deformation-band formation in unconsolidated marine terrace sand, Humboldt County, California. *Geology*, *28*, 111–114. https://doi.org/10.1130/0091-7613(2000)28<111:CADFIU>2.0.CO;2

Chapple, W. M., & Tullis, T. E. (1977). Evalutation of the forces that drive the plates. *Journal of Geophysical Research*, *82*(14), 1967–1984. https://doi.org/10.1029/JB082i014p01967

Chiaraluce, L., Chiarabba, C., Collettini, C., Piccinini, D., & Cocco, M. (2007). Architecture and mechanics of an active low-angle normal fault: Alto Tiberina Fault, northern Appenines, Italy. *Journal of Geophysical Research*, *112*, B10310. https://doi.org/10.1029/2007JB005015

Cooper, A. F., & Norris, R. J. (1994). Anatomy, structural evolution, and slip rate of a plate-boundary thrust: The Alpine Fault at Gaunt Creek, Westland, New Zealand. *Geological Society of America Bulletin*, *106*(5), 627–633. https://doi.org/10.1130/0016-7606(1994)106<0627:ASEASR>2.3.CO;2

De Pascale, G. P., & Langridge, R. M. (2012). New on-fault evidence for a great earthquake in A.D. 1717 central Alpine Fault New Zealand. *Geology*, *40*(9), 791–794. https://doi.org/10.1130/G33363.1

DeMets, C., Gordon, R. G., & Argus, D. F. (2010). Geologically current plate motions. *Geophysical Journal International*, *181*(1), 1–80. https://doi.org/10.1111/j.1365-246X.2009.04491.x

DeMets, C., Gordon, R. G., Argus, D. F., & Stein, S. (1990). Current plate motions. *Geophysical Journal International*, *101*(2), 425–478. https://doi.org/10.1111/j.1365-246X.1990.tb06579.x

Dieterich, J. H. (1972). Time-dependent friction in rocks. *Journal of Geophysical Research*, *77*(20), 3690–3697. https://doi.org/10.1029/JB077i020p03690

Dieterich, J. H. (1979). Modeling of rock friction 1. Experimental results and constitutive equations. *Journal of Geophysical Research*, *84*(B5), 2161–2168. https://doi.org/10.1029/JB084iB05p02161

Dieterich, J. H. (1981). Constitutive properties of faults with simulated gouge. In N. L. Carter, M. Friedman, J. M. Logan, D. W. Stearns (Eds.), *Mechanical behavior of crustal rocks Geophysical Monograph Series 24* (pp. 102–120). Washington, DC: American Geophysical Union. https://doi.org/10.1029/GM024p0103

Dieterich, J. H. (1986). A model for the nucleation of earthquake slip. In S. Das, J. Boatwright, C. H. Scholz (Eds.), *Earthquake source mechanics Geophysical Monograph Series 37* (pp. 37–47). Washington, DC: American Geophysical Union. https://doi.org/10.1029/GM037p0037

Dieterich, J. H. (1992). Earthquake nucleation on faults with rate- and state-dependent strength. *Tectonophysics*, *211*(1–4), 115–134. https://doi.org/10.1016/0040-1951(92)90055-B

Dieterich, J. H., & Kilgore, B. (1994). Direct observation of frictional contacts: New insights for state-dependent properties. *Pure and Applied Geophysics*, *143*(1–3), 283–302. https://doi.org/10.1007/BF00874332

Dieterich, J. H., & Kilgore, B. (1996). Implications of fault constitutive properties for earthquake prediction. *Proceedings of the National Academy of Sciences USA*, *93*(9), 3787–3794. https://doi.org/10.1073/pnas.93.9.3787

Dieterich, J. H., & Linker, M. F. (1992). Fault stability under conditions of variable normal stress. *Geophysical Research Letters*, *19*(16), 1691–1694. https://doi.org/10.1029/92GL01821

Dietz, L. D., & Ellsworth, W. L. (1990). The October 17, 1989, Loma Prieta, California earthquake and its aftershocks: Geometry of the sequence from high-resolution locations. *Geophysical Research Letters*, *17*(9), 1417–1420. https://doi.org/10.1029/GL017i009p01417

Dragert, H., Wang, K., & James, T. S. (2001). A silent slip event on the deeper Cascadia subduction interface. *Science*, *292*(5521), 1525–1528. https://doi.org/10.1126/science.1060152

Ellsworth, W. L., & Beroza, G. C. (1995). Seismic evidence for an earthquake nucleation phase. *Science*, *268*(5212), 851–855. https://doi.org/10.1126/science.268.5212.851

Goldsby, D. L., Rar, A., Pharr, G. M., & Tullis, T. E. (2004). Nanoindentation creep of quartz, with implications for rate- and state-variable friction laws relevant to earthquake mechanics. *Journal of Materials Research*, *19*(1), 357–365. https://doi.org/10.1557/jmr.2004.19.1.357

Griffith, W. A., & Prakash, V. (2015). Integrating field observations and fracture mechanics models to constrain seismic source parameters for ancient earthquakes. *Geology*, *43*, 763–766. https://doi.org/10.1130/G36773.1

Hirose, H., & Obara, K. (2005). Repeating short- and long-terms slow slip events with deep tremor activity around the Bungo channel region, southwest Japan. *Earth, Planets and Space*, *57*(10), 961–972. https://doi.org/10.1186/BF03351875

Hong, T., & Marone, C. (2005). Effects of normal stress perturbations on the frictional properties of simulated faults. *Geochemistry, Geophysics, Geosystems*, *6*, Q03012. https://doi.org/10.1029/2004GC000821

Ide, S., Beroza, G. C., Shelly, D. R., & Uchide, T. (2007). A scaling law for slow earthquakes. *Nature*, *447*(7140), 76–79. https://doi.org/10.1038/nature05780

Ide, S., & Takeo, M. (1997). Determination of constitutive relations of fault slip based on seismic wave analysis. *Journal of Geophysical Research*, *102*(B12), 27,379–27,391. https://doi.org/10.1029/97JB02675

Ikari, M. J. (2019). Laboratory slow slip events in natural geologic materials. *Geophysical Journal International*, *218*(1), 354–387. https://doi.org/10.1093/gji/ggz143

Ikari, M. J., Carpenter, B. M., Kopf, A. J., & Marone, C. (2014). Frictional strength, rate-dependence, and healing in DFDP-1 borehole samples from the Alpine Fault, New Zealand. *Tectonophysics*, *630*, 1–8. https://doi.org/10.1016/j.tecto.2014.05.005

Ikari, M. J., Carpenter, B. M., & Marone, C. (2016). A microphysical interpretation of rate- and state-dependent friction for fault gouge. *Geochemistry, Geophysics, Geosystems*, *17*, 1660–1677. https://doi.org/10.1002/2016GC006286

Ikari, M. J., Carpenter, B. M., Vogt, C., & Kopf, A. J. (2016). Elevated time-dependent strengthening rates observed in San Andreas Fault drilling samples. *Earth and Planetary Science Letters*, *450*, 164–172. https://doi.org/10.1016/j.epsl.2016.06.036

Ikari, M. J., & Kopf, A. J. (2017). Seismic potential of weak, near-surface faults revealed at plate tectonic slip rates. *Science Advances*, *3*(11), e1701269. https://doi.org/10.1126/sciadv.1701269

Ikari, M. J., Marone, C., Saffer, D. M., & Kopf, A. J. (2013). Slip weakening as a mechanism for slow earthquakes. *Nature Geoscience*, *6*(6), 468–472. https://doi.org/10.1038/NGEO1818

Ikari, M. J., Trütner, S., Carpenter, B. M., & Kopf, A. J. (2015). Shear behavior of DFDP-1 borehole samples from the Alpine Fault, New Zealand, under a wide range of experimental conditions. *International Journal of Earth Sciences*, *104*(6), 1523–1535. https://doi.org/10.1007/s00531-014-1115-5

Ito, Y., & Ikari, M. J. (2015). Velocity- and slip-dependent weakening in simulated fault gouge: Implications for multimode fault slip. *Geophysical Research Letters*, *42*, 9247–9254. https://doi.org/10.1002/2015GL065829

Ito, Y., Ikari, M. J., Ujiie, K., & Kopf, A. (2017). Coseismic slip propagation on the Tohoku plate boundary fault facilitated by slip-dependent weakening during slow fault slip. *Geophysical Research Letters*, *44*, 8749–8756. https://doi.org/10.1002/2017GL074307

Kanamori, H. (1986). Rupture processes of subduction-zone earthquakes. *Annual Review of Earth and Planetary Sciences*, *14*(1), 293–322. https://doi.org/10.1146/annurev.ea.14.050186.001453

Karner, S. L., & Marone, C. (2001). Frictional restrengthening in simuated fault gouge: Effect of shear load perturbations. *Journal of Geophysical Research*, *106*(B9), 19,319–19,337. https://doi.org/10.1029/2001JB000263

Kopf, A. (2013). Effective strength of incoming sediments and its implications for plate boundary propagation: Nankai and Costa Rica as type examples of accreting vs. erosive convergent margins. *Tectonophysics*, *608*, 958–969. https://doi.org/10.1016/j.tecto.2013.07.023

Leeman, J. R., Saffer, D. M., Scuderi, M. M., & Marone, C. (2016). Laboratory observations of slow earthquakes and the spectrum of tectonic fault slip modes. *Nature Communications*, *7*(1), 11104. https://doi.org/10.1038/ncomms11104

Linde, A. T., Gladwin, M. T., Johnston, M. J. S., Gwyther, R. L., & Bilham, R. G. (1996). A slow earthquake sequence on the San Andreas Fault. *Nature*, *383*(6595), 65–68. https://doi.org/10.1038/383065a0

Linker, M. F., & Dieterich, J. H. (1992). Effects of variable normal stress on rock friction: Observations and constitutive equations. *Journal of Geophysical Research*, *97*(B4), 4923–4940. https://doi.org/10.1029/92JB00017

Marone, C. (1998a). The effect of loading rate on static friction and the rate of fault healing during the earthquake cycle. *Nature*, *391*(6662), 69–72. https://doi.org/10.1038/34157

Marone, C. (1998b). Laboratory-derived friction laws and their application to seismic faulting. *Annual Review of Earth and Planetary Sciences*, *26*(1), 643–696. https://doi.org/10.1146/annurev.earth.26.1.643

Marone, C., & Kilgore, B. (1993). Scaling of the critical slip distance for seismic faulting with shear strain in fault zones. *Nature*, *362*(6421), 618–621. https://doi.org/10.1038/362618a0

Marone, C., Raleigh, C. B., & Scholz, C. H. (1990). Frictional behavior and constitutive modeling of simulated fault gouge. *Journal of Geophysical Research*, *95*(B5), 7007–7025. https://doi.org/10.1029/JB095iB05p07007

Marone, C., & Saffer, D. M. (2015). The mechanics of frictional healing and slip instability during the seismic cycle. In *Treatise on geophysics* (2nd ed., pp. 111–138). Amsterdam, Netherlands: Elsevier Inc. https://doi.org/10.1016/B978-0-444-53802-4.00092-0

Marone, C., Vidale, J. E., & Ellsworth, W. L. (1995). Fault healing inferred from time dependent variations in source properties of repeating earthquakes. *Geophysical Research Letters*, *22*(22), 3095–3098. https://doi.org/10.1029/95GL03076

Marone, C. J., Scholz, C. H., & Bilham, R. (1991). On the mechanics of earthquake afterslip. *Journal of Geophysical Research*, *96*(B5), 8441–8452. https://doi.org/10.1029/91JB00275

Miller, S. A., Collettini, C., Chiaraluce, L., Cocco, M., Barchi, M., & Klaus, B. J. P. (2004). Aftershocks driven by a high-pressure CO_2 source at depth. *Nature*, *427*(6976), 724–727. https://doi.org/10.1038/nature02251

Miyazaki, S., Segall, P., Fukuda, J., & Kato, T. (2004). Space time distribution of afterslip following the 2003 Tokachi-oki earthquake: Implications for variations in fault zone frictional properties. *Geophysical Research Letters*, *31*, L06623. https://doi.org/10.1029/2003GL019410

Niemeijer, A. R., Boulton, C., Toy, V. G., Townend, J., & Sutherland, R. (2016). Large-displacement, hydrothermal frictional properties of DFDP-1 fault rocks, Alpine Fault, New Zealand: Implications for deep rupture propagation. *Journal of Geophysical Research: Solid Earth*, *121*, 624–647. https://doi.org/10.1002/2015JB012593

Norris, R. J., & Cooper, A. F. (1997). Erosional control on the structural evolution of a transpressional thrust complex on the Alpine Fault, New Zealand. *Journal of Structural Geology*, *19*(10), 1323–1342. https://doi.org/10.1016/S0191-8141(97)00036-9

Norris, R. J., & Cooper, A. F. (2000). Late Quaternary slip rates and slip partitioning on the Alpine Fault, New Zealand. *Journal of Structural Geology*, *23*(2–3), 507–520. https://doi.org/10.1016/S0191-8141(00)00122-X

Ohnaka, M. (2000). A physical scaling relation between the size of an earthquake and its nucleation zone size. *Pure and Applied Geophysics*, *157*(11), 2259–2282. https://doi.org/10.1007/PL00001084

Ohnaka, M. (2003). A constitutive scaling law and a unified comprehension for frictional slip failure, shear fracture of intact rock, and earthquake rupture. *Journal of Geophysical Research*, *108*(B2), 2080. https://doi.org/10.1029/2000JB000123

Okubo, P. G. (1989). Dynamic rupture modeling with laboratory-derived constitutive relations. *Journal of Geophysical Research*, *94*(B9), 12,321–12,335. https://doi.org/10.1029/JB094iB09p12321

Oppenheimer, D. H., Klein, F. W. & Eaton, J. P. (1992). The first 20 years of CALNET, the Northern California Seismic Network, *Open-File Report 92-209*. US Geological Survey, https://doi.org/10.3133/ofr92209

Papageorgiou, A. S., & Aki, K. (1983). A specific barrier model for the quantitative description of inhomogeneous faulting and the prediction of strong ground motion. Part II. Applications of the model. *Bulletin of the Seismological Society of America*, *73*, 953–978.

Peng, Z., & Gomberg, J. (2010). An integrated perspective of the continuum between earthquakes and slow-slip phenomena. *Nature Geoscience*, *3*(9), 599–607. https://doi.org/10.1038/NGEO940

Perfettini, H., & Avouac, J.-P. (2004). Postseismic relaxation driven by brittle creep: A possible mechanism to reconcile geodetic measurements and the decay rate of aftershocks, application to the Chi-Chi earthquake, Taiwan. *Journal of Geophysical Research*, *109*, B02304. https://doi.org/10.1029/2003JB002488

Perfettini, H., & Avouac, J.-P. (2007). Modeling afterslip and aftershocks following the 1992 Landers earthquake. *Journal of Geophysical Research*, *112*, B07409. https://doi.org/10.1029/2006JB004399

Perfettini, H., Avouac, J.-P., Tavera, H., Kositsky, A., Nocquet, J.-M., Bondoux, F., et al. (2010). Seismic and aseismic slip on the Central Peru megathrust. *Nature*, *465*(7294), 78–81. https://doi.org/10.1038/nature09062

Prescott, W. H., & Burford, R. O. (1976). Slip on the Sargent fault. *Bulletin of the Seismological Society of America*, *66*, 1013–1016.

Reinen, L. A., & Weeks, J. D. (1993). Determination of rock friction constitutive parameters using an iterative least-squares inversion method. *Journal of Geophysical Research*, *98*(B9), 15,937–15,950. https://doi.org/10.1029/93JB00780

Reinen, L. A., Weeks, J. D., & Tullis, T. E. (1994). The frictional behavior of lizardite and antigorite serpentinites: Experiments, constitutive models, and implications for natural faults. *Pure and Applied Geophysics*, *143*, 317–358. https://doi.org/10.1007/BF00874334

Richardson, E., & Marone, C. (1999). Effects of normal stress vibrations on frictional healing. *Journal of Geophysical Research*, *104*(B12), 28,859–28,878. https://doi.org/10.1029/1999JB900320

Roy, M., & Marone, C. (1996). Earthquake nucleation on model faults with rate- and state-dependent friction: Effects of inertia. *Journal of Geophysical Research*, *101*(B6), 13,919–13,932. https://doi.org/10.1029/96JB00529

Ruina, A. L. (1983). Slip instability and state variable friction laws. *Journal of Geophysical Research*, *88*(B12), 10,359–10,370. https://doi.org/10.1029/JB088iB12p10359

Ryan, K. L., Riviére, J., & Marone, C. (2018). The role of shear stress in fault healing and frictional aging. *Journal of Geophysical Research: Solid Earth*, *123*, 10,479–10,495. https://doi.org/10.1029/2018JB016296

Ryder, I., & Bürgmann, R. (2008). Spatial variations in slip deficit on the central San Andreas Fault. *Geophysical Journal International*, *175*(3), 837–852. https://doi.org/10.1111/j.1365-246X.2008.03938.x

Saffer, D. M., & Marone, C. (2003). Comparison of smectite- and illite-rich gouge frictional properties: Application to the updip limit of the seismogenic zone along subduction megathrusts. *Earth and Planetary Science Letters*, *215*(1–2), 219–235. https://doi.org/10.1016/S0012-821X(03)00424-2

Scholz, C. H. (1998). Earthquakes and friction laws. *Nature*, *391*(6662), 37–42. https://doi.org/10.1038/34097

Segall, P., Bürgmann, R., & Matthews, M. (2000). Time-dependent triggered afterslip following the 1989 Loma Prieta earthquake. *Journal of Geophysical Research*, *105*(B3), 5615–5634. https://doi.org/10.1029/1999JB900352

Sibson, R. H. (1989). Earthquake faulting as a structural process. *Journal of Structural Geology*, *11*(1–2), 1–14. https://doi.org/10.1016/0191-8141(89)90032-1

Skarbek, R. M., & Savage, H. M. (2019). RSFit3000: A MATLAB GUI-based program for determining rate and state frictional parameters from experimental data. *Geosphere*, *15*(5), 1665–1676. https://doi.org/10.1130/GES02122.1

Sleep, N. H. (2005). Physical basis of evolution laws for rate and state friction. *Geochemistry, Geophysics, Geosystems*, *6*, Q11008. https://doi.org/10.1029/2005GC000991

Sleep, N. H. (2006). Real contacts and evolution laws for rate and state friction. *Geochemistry, Geophysics, Geosystems*, *7*, Q08012. https://doi.org/10.1029/2005GC001187

Sleep, N. H. (2012). Microscopic elasticity and rate and state friction evolution laws. *Geochemistry, Geophysics, Geosystems*, *13*, Q12002. https://doi.org/10.1029/2012GC004393

Sutherland, R., Berryman, K., & Norris, R. (2006). Quaternary slip rate and geomorphology of the Alpine Fault: Implications for kinematics and seismic hazard in southwest New Zealand. *Geological Society of America Bulletin*, *118*(3–4), 464–474. https://doi.org/10.1130/B25627.1

Sutherland, R., Eberhart-Phillips, D., Harris, R. A., Stern, T., Beavan, J., Ellis, S., et al. (2007). Do great earthquakes occur on the Alpine Fault in central South Island, New Zealand? In D. Okaya, T. Stern, F. Davey (Eds.), *A Continental Plate Boundary: Tectonics at South Island, New Zealand*, *Geophysical Monograph Series 175* (pp. 235–251). Washington, DC: American Geophysical Union. https://doi.org/10.1029/175GM12

Sutherland, R., Toy, V. G., Townend, J., Cox, S. C., Eccles, J. D., Faulkner, D. R., et al. (2012). DFDP-1 drilling, Alpine Fault, New Zealand, reveals influence of fluids on architecture and rupture of faults. *Geology*, *40*(12), 1143–1146. https://doi.org/10.1130/G33614.1

Szeliga, W., Melbourne, T., Santillan, M., & Miller, M. (2008). GPS constraints on 34 slow slip events within the Cascadia subduction zone, 1997–2005. *Journal of Geophysical Research*, *113*, B04404. https://doi.org/10.1029/2007JB004948

Teufel, L. W. (1981). Pore volume changes during frictional sliding of simulated faults. In N. L. Carter, M. Friedman, J. M. Logan, D. W. Stearns (Eds.), *Mechanical behavior of crustal rocks*, *Geophysical Monograph Series 24* (pp. 135–145). Washington, DC: American Geophysical Union. https://doi.org/10.1029/GM024p0135

Titus, S. J., DeMets, C., & Tikoff, B. (2005). New slip rate estimates for the creeping segment of the San Andreas Fault, California. *Geology*, *33*(3), 205–208. https://doi.org/10.1130/G21107.1

Townend, J., Sutherland, R., & Toy, V. (2009). Deep Fault Drilling Project—Alpine Fault, New Zealand. *Scientific Drilling*, *8*, 75–82. https://doi.org/10.2204/iodp.sd.8.12.2009

Toy, V. G., Boulton, C. J., Sutherland, R., Townend, J., Norris, R. J., Little, T. A., et al. (2015). Fault rock lithologies and architecture of the central Alpine Fault, New Zealand, revealed by DFDP-1 drilling. *Lithosphere*, *7*(2), 155–173. https://doi.org/10.1130/L395.1

Vidale, J. E., Ellsworth, W. L., Cole, A., & Marone, C. (1994). Variations in rupture process with recurrence interval in a repeated small earthquake. *Nature*, *368*(6472), 624–626. https://doi.org/10.1038/368624a0

Vogt, C., Lauterjung, J., & Fischer, R. (2002). Investigation of the clay fraction (< 2 μm) of the Clay Minerals Society reference clays. *Clays and Clay Minerals*, *50*(3), 388–400. https://doi.org/10.1346/000986002760833765

Wells, A., Yetton, M. D., Duncan, R. P., & Stewart, G. H. (1999). Prehistoric dates of the most recent Alpine Fault earthquakes, New Zealand. *Geology*, *27*, 995–998. https://doi.org/10.1130/0091-7613(1999)027<0995:PDOTMR>2.3.CO;2

Working Group on California Earthquake Probabilities (1999). Earthquake probabilities in the San Francisco Bay region: 2000 to 2030—A summary of findings, U.S. Geological Survey Open File Report, 99–517, https://doi.org/10.3133/3ofr99517